Criterion for traffic phases in single vehicle data and empirical test of a microscopic three-phase traffic theory

2006 J. Phys. A: Math. Gen. 39 2001

(http://iopscience.iop.org/0305-4470/39/9/002)

INSTITUTE OF PHYSICS PUBLISHING JOURNAL OF PHYSICS A: MATHEMATICAL AND GENERAL

J. Phys. A: Math. Gen. **39** (2006) 2001–2020 doi:10.1088/0305-4470/39/9/002

Criterion for traffic phases in single vehicle data and empirical test of a microscopic three-phase traffic theory

Boris S Kerner[1], **Sergey L Klenov**[2] **and Andreas Hiller**[1]

[1] DaimlerChrysler AG, REI/VF, HPC: G021, 71059 Sindelfingen, Germany
[2] Moscow Institute of Physics and Technology, Department of Physics, 141700 Dolgoprudny, Moscow Region, Russia

Received 25 July 2005, in final form 14 December 2005
Published 15 February 2006
Online at stacks.iop.org/JPhysA/39/2001

Abstract

Based on empirical and numerical microscopic analyses, the physical nature of a qualitatively different behaviour of the wide moving jam phase in comparison with the synchronized flow phase—microscopic traffic flow interruption within the wide moving jam phase—is found. A microscopic criterion for distinguishing the synchronized flow and wide moving jam phases in single vehicle data measured at a single freeway location is presented. Based on this criterion, empirical microscopic classification of different local congested traffic states is performed. Simulations made show that the microscopic criterion and macroscopic spatiotemporal objective criteria lead to the same identification of the synchronized flow and wide moving jam phases in congested traffic. Microscopic models in the context of three-phase traffic theory have been tested based on the microscopic criterion for the phases in congested traffic. It is found that microscopic three-phase traffic models can explain both microscopic and macroscopic empirical congested pattern features. It is obtained that microscopic frequency distributions for vehicle speed difference as well as fundamental diagrams and speed correlation functions can depend on the spatial co-ordinate considerably. It turns out that microscopic optimal velocity (OV) functions and time headway distributions are not necessarily qualitatively different, even if local congested traffic states are qualitatively different. The reason for this is that important *spatiotemporal* features of congested traffic patterns are *lost* in these as well as in many other macroscopic and microscopic traffic characteristics, which are widely used as the empirical basis for a test of traffic flow models, specifically, cellular automata traffic flow models.

PACS numbers: 47.54.+r, 64.60.Cn, 64.60.Lx, 89.40.+k

1. Introduction

Freeway traffic is a complex dynamic process, in which complex spatiotemporal congested patterns are observed. From spatiotemporal analysis of measured data, it has been found that there are two different phases in congested traffic, synchronized flow and wide moving jam (see references in the book [1]). Thus, there are three-traffic phases: (1) free flow; (2) synchronized flow; (3) wide moving jam.

In congested traffic, the following macroscopic spatiotemporal objective (empirical) criteria *define* the synchronized flow and wide moving jam phases [1]. The wide moving jam is a moving jam that exhibits the *characteristic, i.e., unique and coherent feature* to maintain the mean velocity of the downstream jam front. The jam exhibits this feature even when the jam propagates through any other traffic states or freeway bottlenecks. In contrast, synchronized flow does not exhibit this characteristic feature, in particular, the downstream front of synchronized flow is often *fixed* at a freeway bottleneck. These criteria are associated with *spatiotemporal propagation* features of congested traffic. The features cannot be found in traffic measurements of traffic characteristics (like optimal velocity (OV) functions, time headway distributions, fundamental diagrams, etc) made at a single freeway location.

Congested traffic, which occurs at freeway bottlenecks, exhibits the following fundamental empirical features [1].

(i) The onset of congestion at a bottleneck is associated with a local phase transition from free flow to synchronized flow. This F $\rightarrow$ S transition is a first-order phase transition and exhibits probabilistic nature.
(ii) There can be spontaneous and induced F $\rightarrow$ S transitions at a freeway bottleneck.
(iii) Wide moving jams can emerge spontaneously only in synchronized flow (S $\rightarrow$ J transition), i.e., due to F $\rightarrow$ S $\rightarrow$ J transitions.
(iv) There are two main types of congested patterns at an isolated bottleneck: a synchronized flow pattern (SP) and a general pattern (GP). An SP consists of synchronized flow only, i.e., no wide moving jams emerge in the SP. A GP is a congested pattern, which consists of synchronized flow upstream of the bottleneck and wide moving jams that emerge spontaneously in this synchronized flow.

To explain the complex dynamic process of freeway traffic, a huge number of traffic flow models have been introduced (see the reviews [2–8], the book [1] and the conference proceedings [9–12]).

Past traffic flow models reviewed in [2–7] cannot explain and predict the spatiotemporal features (i)–(iv) of traffic mentioned above. The only one exception is the characteristic features of wide moving jam propagation that can be shown in some of these models [1]. To explain features (i)–(iv), Kerner introduced a three-phase traffic theory [13, 14]. This is the basis of recent microscopic three-phase traffic models [15–22].

Microscopic theory [15–18] explains macroscopic spatiotemporal congested pattern phenomena (i)–(iv). We can expect that these models can also explain various single vehicle (i.e., microscopic) traffic flow characteristics. However, single vehicle data measured at many different freeway locations, which can be sufficient for a reliable spatiotemporal analysis of whole congested pattern structures, are not available.

In this paper, a microscopic empirical criterion for the synchronized flow and wide moving jam phases is found, which enables us to distinguish the phases in empirical single vehicle data measured at a *single* freeway location. Based on the microscopic criterion, microscopic models of [15–18] are tested. It is found that the phases identified by the microscopic criterion satisfy also the macroscopic spatiotemporal objective criteria, which define the synchronized

flow and wide moving jam phases. In a test of a microscopic three-phase traffic theory, firstly spatiotemporal congested pattern evolution under time dependence of traffic demand taken from empirical results is modelled. Then congested pattern characteristics associated with different locations within the patterns are numerically studied and compared with empirical results. The paper is organized as follows. Empirical findings are considered in section 2. In section 3, microscopic and macroscopic congested pattern characteristics found in numerical simulations are compared with empirical results.

2. Empirical results

2.1. Congested states in single vehicle data

Single vehicle characteristics are usually obtained either in driver experiments or through the use of detectors (e.g., [23–32]). In the latter case, data from a single freeway location or aggregated data measured at different locations are used. For empirical tests of traffic flow models time headway distributions (probability density for different time headways) and optimal velocity (OV) functions (the mean speed as a function of space gap between vehicles at a given density) are often used (e.g., [25]).

Single vehicle data used in the paper have been measured on a two-lane section of the freeway A92-West (Germany) at detectors D1 and D2 between intersections 'AS Freising-Süd' (I2) and AK Neufahrn' (I3) near Munich Airport (intersection I1: AS Flughafen' in figure 1(*a*)). For an overview of congested states observed in single vehicle data and used below, the data averaged over 1 min intervals are shown in figure 1(*b*)–(*e*).

Single vehicle data are measured through the use of two sets of double induction loop detectors. A detector set consists of two detectors for each of the freeway lanes. A detector registers a vehicle by producing a current electric pulse whose duration Δt_i is related to the time taken by the vehicle to traverse the induction loop. This enables us to calculate the gross time gap (gross time headway) between two vehicles i and $i+1$ that have passed the loop one after the other $\tau_{i,i+1}^{(\mathrm{gross})}$. There are two detector loops in each detector. The distance between these loops is constant. This enables us to calculate the individual vehicle speed v_i and estimate the vehicle length $d_i = v_i \Delta t_i$ as well as the net time gap (time headway) between the vehicles i and $i+1$: $\tau_{i,i+1} = \tau_{i,i+1}^{(\mathrm{gross})} - \Delta t_i$.

If in examples shown in figure 1(*c*)–(*e*) there are moving jams, then these jams should be narrow moving jams, i.e., these examples should correspond to the synchronized flow phase. Indeed, during the whole time of congested traffic existence there are no drops in the flow rate, which are typical for wide moving jams [1]. In contrast, there are short-time drops both in the average speed and flow rate in figure 1(*b*)). Such drops are typical for wide moving jams. However, from these *macroscopic* data measured at a single location only we cannot make a conclusion with certainty whether these drops are associated with the wide moving jam phase or not. Nevertheless, this conclusion can be made if the microscopic criterion for the traffic phases presented below is applied.

2.2. Traffic flow interruption effect as microscopic criterion for wide moving jam

The spatiotemporal criteria for a wide moving jam—jam propagation through a bottleneck while maintaining the downstream jam front velocity—which distinguish the wide moving jam and synchronized flow, can be explained by a traffic flow discontinuity within a wide moving jam. Traffic flow is interrupted by the wide moving jam: there is no influence of the inflow into the jam on the jam outflow. For this reason, the mean downstream jam front

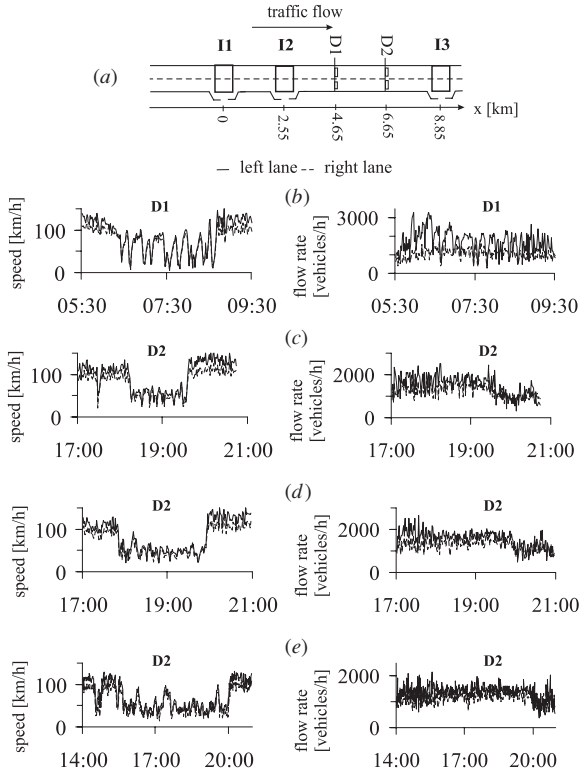

Figure 1. Macroscopic characteristics of empirical single vehicle data measured on the freeway A92-West. (*a*) Sketch of detector arrangement of a section on the freeway A92-West. (*b*)–(*e*) Local traffic dynamics (1 min average data) of the speed (left) and flow rate (right) on four different days in both freeway lanes; 17 July, 2000 (*b*), 23 August, 2000 (*c*), 27 July, 2000 (*d*) and 03 August, 2000 (*e*).

velocity and the jam outflow exhibit fundamental characteristic features, which do not depend on the jam inflow [1]. A difference between the jam inflow and the jam outflow changes the jam width only. This *traffic flow interruption effect* is a general effect for each wide moving jam.

The jam outflow becomes independent of the jam inflow, when the traffic flow interruption effect within a moving jam occurs. In a hypothetical case, when all vehicles within a moving jam do not move, the criterion for the traffic flow interruption effect is

$$I = \frac{\tau_{\mathrm{J}}}{\tau_{\mathrm{del}}^{(\mathrm{ac})}} \gg 1, \tag{1}$$

where τ_{J} is the jam duration, i.e., the time interval between the upstream and downstream jam fronts passing a detector location and $\tau_{\mathrm{del}}^{(\mathrm{ac})}$ is the mean time delay in vehicle acceleration at the downstream jam front from a vehicle standstill; $\tau_{\mathrm{del}}^{(\mathrm{ac})}$ determines the jam outflow; I is approximately equal to the vehicle number stopped within the jam. Note that corresponding to empirical results $\tau_{\mathrm{del}}^{(\mathrm{ac})} \approx 1.5$–$2$ sec [1].

In real traffic, vehicles come to a stop at very different distances to one another when they meet a wide moving jam. Then the vehicles begin to cover these blanks within the jam. As

a result, low speed states appear associated with upstream moving blanks within the jam (see section 11.2.4 in [1]). A *sufficient* criterion for flow interruption is

$$I_s = \frac{\tau_{max}}{\tau_{del}^{(ac)}} \gg 1, \tag{2}$$

where τ_{max} is the maximum time headway between two vehicles within the jam ($\tau_{max} \leqslant \tau_J$). Under the condition (2), there are at least several vehicles within the jam that are in a standstill or if they are still moving, it is only with a low speed in comparison with the speed in the jam inflow and outflow. These vehicles separate vehicles accelerating at the downstream jam front from vehicles decelerating at the upstream jam front: the jam outflow does not depend on the jam inflow. As a result, the mean downstream jam front velocity is equal to $v_g = -1/\left(\tau_{del}^{(ac)}\rho_{max}\right)$ [1] (ρ_{max} is the average density within the jam just upstream of the downstream jam front) regardless of whether there are bottlenecks or other complex traffic states on the freeway. In other words, this jam propagates through a bottleneck while maintaining the mean downstream jam front velocity v_g. In accordance with the macroscopic objective spatiotemporal criteria for the traffic phases in congested traffic (section 1), this jam is a wide moving jam. Thus, we can assume that the traffic flow interruption effect can be used as a criterion to distinguish the synchronized flow and wide moving jam phases in single vehicle data. This is possible even if data are measured at a single freeway location.

The interruption of traffic flow within a moving jam in the left and right lanes (on the graph of the vehicle speed in figure 2(*a*)) can clearly be seen in the time dependences of time headways τ (time headways about 20 s and 30 s in the left and right lanes, respectively in figure 2(*b*)) and of the value $3600/\tau^{(gross)}$ (figure 2(*c*)). Before and after the jam has passed detector D1 (due to the jam upstream propagation) there are many vehicles that traverse the detector. Within the jam, during two time intervals (labelled 'flow interruption' in figure 2(*c*)) there are no vehicles traversing the detector, when the speed within the jam is approximately zero (figure 2(*a*)). This means that traffic flow is discontinuous within the moving jam, i.e., this moving jam is associated with the wide moving jam phase. Later, some vehicles within the jam have time headways of about 4 s or longer associated with moving blanks.

In figure 1(*c*)–(*e*), there also are many moving jams during periods of congested traffic. For example, the speed within two moving jams in figure 2(*d*) is also very low. In contrast with the wide moving jam in figure 2(*a*), these moving jams should be classified as narrow moving jams, which are associated with the synchronized flow phase [1] (see also explanations in section 3.1). This is because there are no traffic flow interruptions within these moving jams (figure 2(*d*)–(*f*)). Indeed, upstream, downstream of the jams, and within the jams there are many vehicles that traverse the detector: there is no qualitative difference in the time dependences of time headways for different time intervals associated with these narrow jams and in traffic flow upstream or downstream of the jams (figure 2(*e*)).

This can be explained if it is assumed that each vehicle, which meets a narrow moving jam, can nevertheless accelerate later almost without any time delay within the jam. Within the upstream front vehicles must decelerate to a very low speed (sometimes as low as zero). However, they can accelerate almost immediately at the downstream jam front. These assumptions are confirmed by single vehicle data shown in figure 2(*e*), (*f*), in which time intervals between different measurements of time headways and for the value $3600/\tau^{(gross)}$ for different vehicles exhibit the same behaviour away and within the jams. Even if within a narrow moving jam there are vehicles that are stopped, the condition

$$I_s \sim 1 \tag{3}$$

can be satisfied. Under this condition, there is no flow interruption within this jam. In other words, in contrast with a wide moving jam, there is no drop in flow rate within a narrow

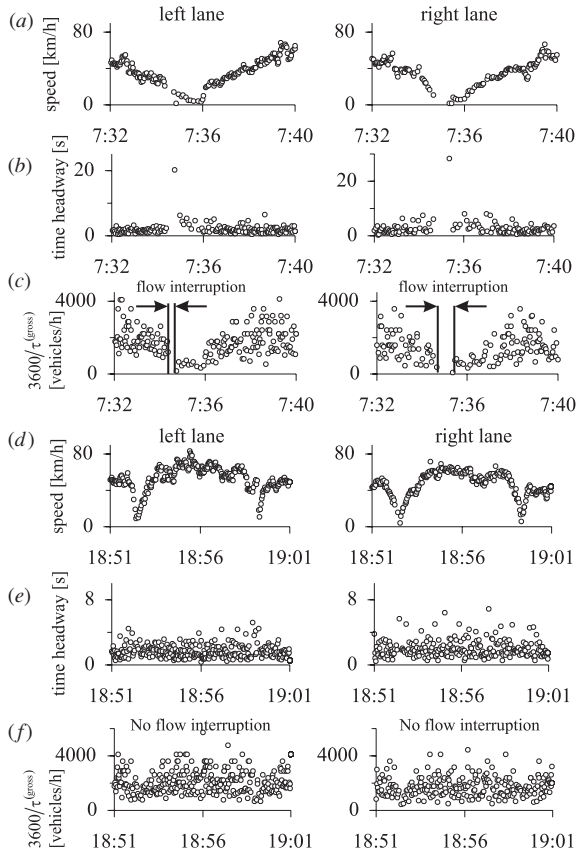

Figure 2. Microscopic criterion for wide moving jam. (*a*)–(*c*) Empirical single vehicle data for speed within a wide moving jam (*a*) in the left (left figures) and right lanes (right figures) as well as the associated time distributions of time headways τ (*b*) and the value $3600/\tau^{(\mathrm{gross})}$ (*c*) related to figure 1 (*b*). (*d*)–(*f*) Empirical single vehicle data for speed within a sequence of two narrow moving jams (*d*) in the left (left figures) and right lanes (right figures) as well as the associated time distributions of τ (*e*) and $3600/\tau^{(\mathrm{gross})}$ (*f*) related to figure 1(*c*).

moving jam. Thus, regardless of these narrow moving jams traffic flow is not discontinuous, i.e., the narrow moving jams are associated with the synchronized flow phase.

This single vehicle analysis enables us to conclude that congested traffic in figure 1(*b*) is associated with a sequence of wide moving jams. In contrast, congested traffic in figure 1(*c*)–(*e*) is associated with different states of the synchronized flow phase.

In common speech, the term a 'stop-and-go wave' is used in context with intervals of low or zero speed in traffic flow. However, this is not necessarily equivalent to flow interruption described above. For a driver a sequence of narrow moving jams can also be considered 'stop-and-go waves'. This is because within a narrow moving jam during a short time interval $\Delta t \sim \tau_{\mathrm{del}}^{(\mathrm{ac})}$ the driver can be stopped. However, the sequence of narrow moving jams is associated with the synchronized flow phase, rather than with the wide moving jam phase. Moreover, 'stop-and-go waves' can be associated with qualitatively different complex spatiotemporal sequences of various traffic phases and states. For example, 'stop-and-go wave' can be (i) a sequence of the wide moving jam and free flow phases, (ii) a sequence of the wide moving jam, free flow, and synchronized flow phases, (iii) a sequence of the free flow

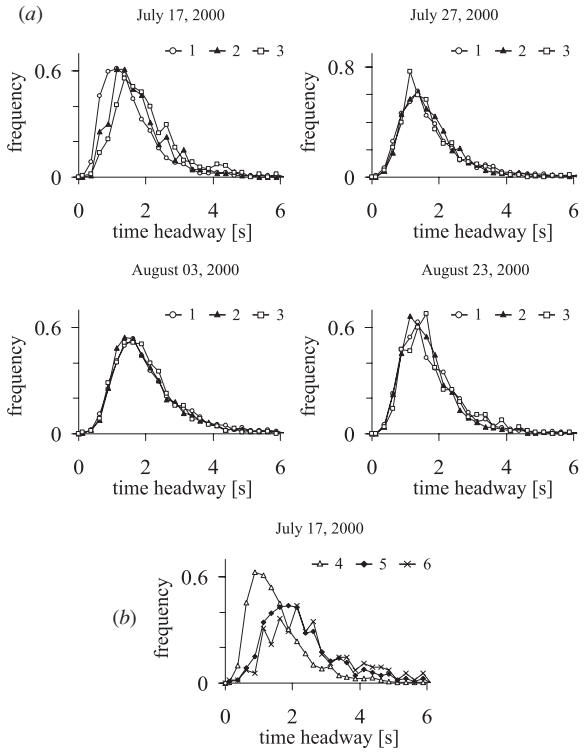

Figure 3. Empirical time headway distributions for different density ranges; (*a*) curve 1: $20 < \rho < 30$; curve 2: $30 < \rho < 40$; curve 3: $40 < \rho < 50$ vehicles/km. (*b*) Time headway distributions associated with the example in figure 1(*b*) for different speed ranges: curve 4: $v > 50$, curve 5: $v < 30$; curve 6: $v < 20$ km h^{-1}. Left lane.

and synchronized flow phases, if there are narrow moving jams in the synchronized flow, or (iv) synchronized flow containing narrow moving jams. For these reasons, we do not use the term 'stop-and-go wave'.

2.3. Time headway distributions and optimal velocity (OV) functions

Although local traffic dynamics in figure 1(*b*) is qualitatively different from figure 1(*c*)–(*e*), the related time headway distributions found for different density ranges are qualitatively the same (figure 3(*a*)). Moreover, these distributions are both qualitatively and even approximately quantitatively the same as those found for congested traffic on different freeways in various countries (e.g. [29, 23, 30, 24]). However, in the example shown in figure 1(*b*), time headway distributions for vehicle speeds $v > 50$ km h^{-1}, $v < 30$ km h^{-1} and $v < 20$ km h^{-1} drawn separately exhibit a shift to longer time headways (figure 3(*b*)); in average, the lower the speed, the more the distributions are shifted. Due to moving blanks within wide moving jams vehicles within the jams exhibit appreciable longer time headways, which are the longer, the lower the speed. However, such time headways shift can also be observed in synchronized flow in which no wide moving jams propagate. It must be stressed that even these differences in the time headway distributions do not permit traffic phase distinguishing in space and time. They say nothing about spatiotemporal alternations of the synchronized flow and wide moving

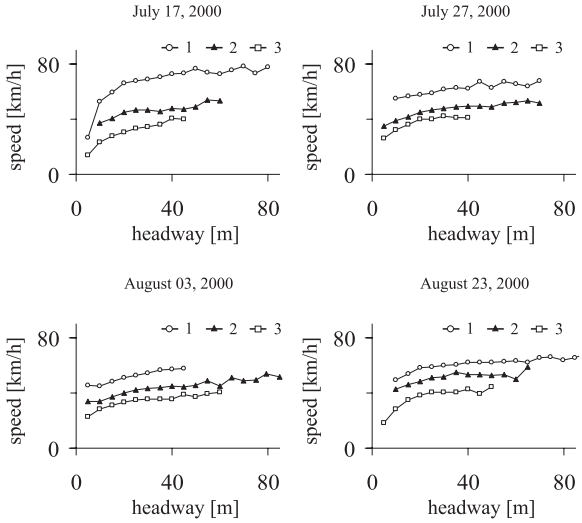

Figure 4. Empirical OV functions for different density ranges: curves 1–20$< \rho <$ 30, curves 2–30$< \rho <$ 40, curves 3–40$< \rho <$ 50 vehicles/km. Left lane.

jam phases, jam duration, time intervals between jams, speed distributions between the jams and other spatiotemporal congested traffic characteristics.

OV functions are space gap (headway) dependences of the mean vehicle speed calculated for different given density ranges [23–25]. The OV functions found do not exhibit some qualitative differences for different local congested traffic dynamics (figure 4). They are qualitatively the same as the OV functions first derived for aggregated single vehicle data in [23]: at smaller headways the speed increases with space headways considerably, whereas for larger space headways there is a saturation effect for the speed growth. Thus, in OV functions many of the spatiotemporal traffic characteristics are averaged.

We can conclude that known time headway distributions and OV functions [23–25] cannot be used for clear distinguishing the phases in spatiotemporal congested patterns. In contrast, if the criterion (2) in congested traffic of low speed is satisfied, then the traffic phase is definitely the wide moving jam phase, i.e., this criterion is superior than time headway distributions and OV functions for traffic phase identification.

3. Simulation results

In numerical simulations presented below, we use stochastic microscopic models and model parameters of [17, 18] and the KKW cellular automata (CA) model of [16]. A detailed consideration of the models, their physics and parameters can be found in sections 16.2, 16.3 and 20.2 of the book [1]. When some other model parameters are used, they are given in figure captions. The main idea of these models is the speed adaptation effect in synchronized flow that takes place when the vehicle cannot pass the preceding vehicle. Within a so-called 'synchronization gap', the vehicle tends to adjust its speed to preceding vehicle without caring, what the precise space gap is, as long as it is safe. To simulate driver behaviour in various traffic conditions, acceleration and deceleration delays depend on whether a vehicle currently decelerates or accelerates as well as on the vehicle speed.

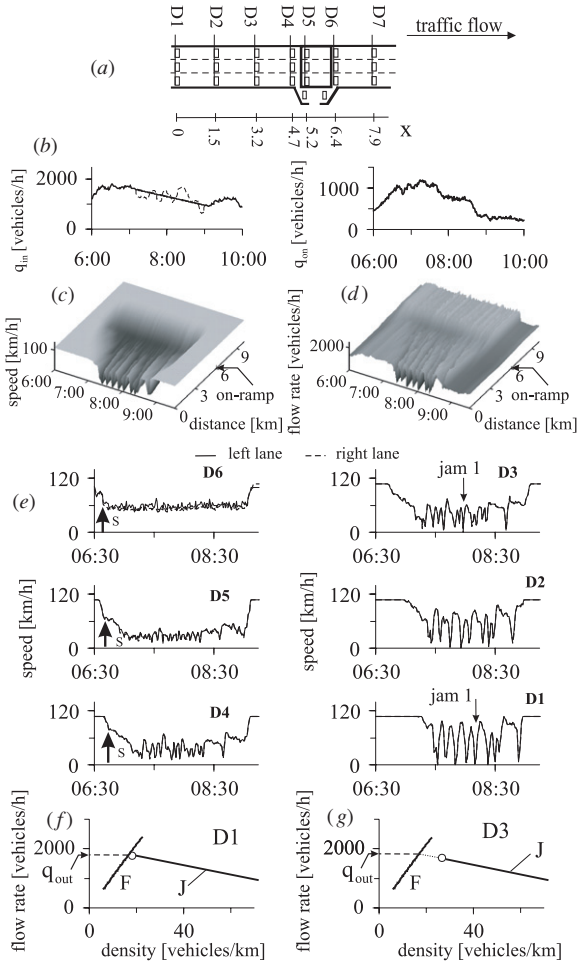

Figure 5. Simulation of GP evolution. (*a*) Sketch of freeway section. (*b*) Time dependences of flow rates on the main road upstream of the on-ramp q_{in} and to the on-ramp q_{on}. (*c*), (*d*) Speed (*c*) and flow rate (*d*) averaged across the road in space and time for spontaneous GP emergence and evolution. (*e*) Speed at different detectors as a function of time for the GP. (*f*, *g*)—The line *J* when free flow (*f*) and synchronized flow (*g*) is formed at two different detector locations in the wide moving jam outflow for the wide moving jam labelled 'jam 1' within the GP in (*e*). q_{out} is the flow rate in free flow formed by the wide moving jam outflow. Arrows *S* show an F $\rightarrow$ S transition at the bottleneck. At the upstream boundary of the main road, $q_{\text{in}}(t)$ associated with empirical data measured at D1 has been applied; as wide moving jams are observed during 7:15–9:00 at D1, $q_{\text{in}}(t)$ is approximated by a line. $q_{\text{on}}(t)$ is taken from measurements in the on-ramp lane. Model of identical vehicles of section 16.3 of [1].

Two pattern formation scenarios have been chosen. In these scenarios, empirical time dependence of traffic demand and drivers' destinations (whether a vehicle leaves the main road to an off-ramp or it further follows the main road) associated with empirical macroscopic patterns are used in model simulations at the upstream model boundaries of the main road and of an on-ramp. At downstream model boundary conditions for vehicle freely leaving a modelling freeway section(s) are given. Then spatiotemporal congested patterns emerge, develop and dissolve in this freeway model with the same types of bottlenecks as those in empirical observations.

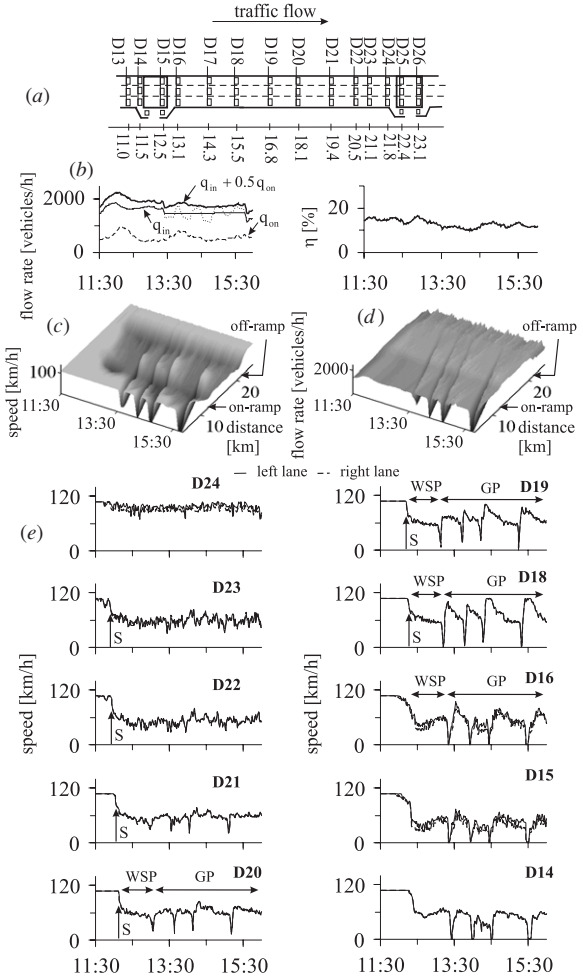

Figure 6. Simulations of congested pattern evolution at two adjacent bottlenecks. (*a*) Sketch of freeway section. (*b*) Time dependences of flow rates $q_{\rm in}$, $q_{\rm on}$ and the percentage of vehicles η that leave the main road to the off-ramp. (*c*, *d*) Speed (*c*) and flow rate (*d*) averaged across the road in space and time. (*e*) Speed at different detectors as a function of time. $v_{\rm free\,off} = 65$ km h^{-1}. Arrows *S* show an F $\rightarrow$ S transition at the off-ramp bottleneck. Time intervals labelled WSP and GP show durations of WSP and GP existence upstream of the off-ramp bottleneck. At the road upstream boundary, $q_{\rm in}(t)$ is taken from empirical data. $q_{\rm on}(t)$ is taken from measurements in the on-ramp lane. The empirical flow rate to the off-ramp $q_{\rm off}(t)$ is used to calculate $\eta(t)$ in (*b*). Model of identical vehicles of section 16.3 of [1].

In the first scenario, empirical data for general pattern (GP) emergence at an on-ramp bottleneck (figure 12.5 of [1]) are compared with GP simulation (figure 5). A model of two-lane freeway with the bottleneck in which detector locations D1–D6 are the same as those in empirical data is applied (figure 5(*a*)). It turns out that GP emergence and evolution (figure 5(*c*)–(*e*)) are qualitatively and quantitatively the same as those in empirical observations (figure 12.5 of [1]) [33].

In the second scenario, empirical data for widening synchronized flow pattern (WSP) emergence at an off-ramp bottleneck with subsequent WSP transformation into an GP and an

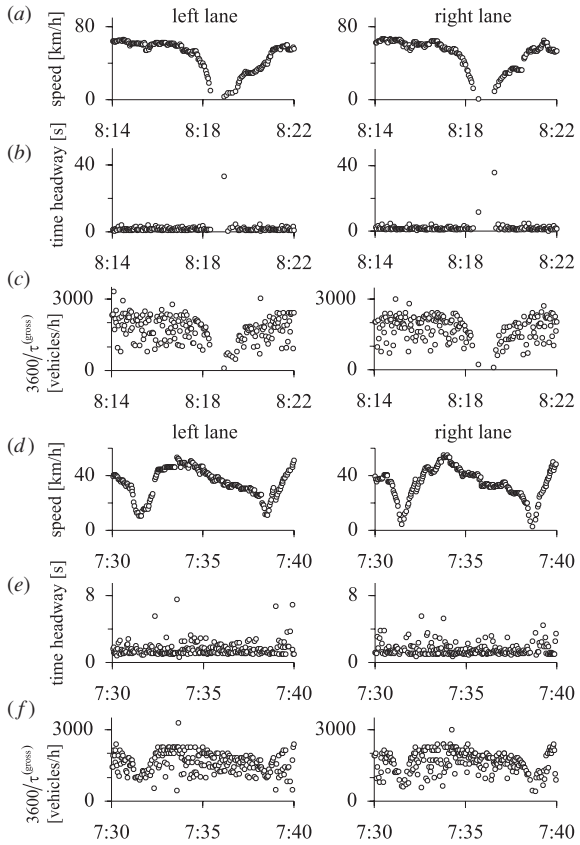

Figure 7. Simulations of the microscopic traffic flow interruption effect and the criterion for traffic phase identification in different local microscopic congested traffic states related to different locations within the GP shown in figure 5(*c*)–(*e*). (*a*)–(*c*) Single vehicle data in the left (left) and in right lanes (right) at the location D2 for speed within a wide moving jam (*a*), the associated time distributions of time headways τ (*b*) and of $3600/\tau^{(\mathrm{gross})}$ (*c*). (*d*)–(*f*) Single vehicle data in the left (left) and in right lanes (right) at the location D4 for speed within a sequence of two narrow moving jams (*d*) and the associated time distributions of τ (*e*) and of $3600/\tau^{(\mathrm{gross})}$ (*f*).

expanded congested pattern (EP) at an on-ramp bottleneck (figures 9.14 and 14.1 of [1]) are compared with simulation results. A model of two-lane freeway with on-ramp and off-ramp bottlenecks in which detector locations D13–D26 are the same as those in empirical data is applied (figure 6(*a*)). It turns out that congested pattern emergence and evolution (figure 6(*c*)–(*e*)) are qualitatively the same as those in empirical observations (figures 9.14 and 14.1 of [1]) [33].

Based on these scenarios, a proof of the microscopic criterion for the traffic phases (section 3.1) and an empirical test of congested pattern characteristics of microscopic three-phase traffic theory (section 3.2) are performed.

3.1. Proof of microscopic criterion for wide moving jam

The microscopic criterion (2) enables us to distinguish clearly the wide moving jam and synchronized flow phases in single vehicle data associated with moving jams in figures 5(*c*)–(*e*)

and 6(*c*)–(*e*). Indeed, in figure 7 the same dependences and characteristics as those in empirical results (figure 2) are found for a wide moving jam (figure 7(*a*)–(*c*)) and two narrow moving jams (figure 7(*d*)–(*f*)) associated with two different local microscopic congested states related to two locations within the GP in figure 5(*c*)–(*e*). If the microscopic criterion is applied for the moving jams, which propagate through the on-ramp bottleneck in figure 6(*c*)–(*e*), then we find that within each of these jams traffic interruption occurs, i.e., the condition (2) is satisfied. This means that corresponding to the microscopic criterion these moving jams are wide moving jams. The same conclusion is made from the macroscopic spatiotemporal objective criteria for traffic phases. Indeed, these jams propagate through the bottleneck while maintaining the mean jam downstream front velocity. Thus, at least in the cases of wide moving jams within the GP (figure 5) and EP (figure 6) the microscopic criterion and macroscopic objective spatiotemporal criteria for the traffic phases lead to the same result of phase identification in congested traffic.

To prove the latter conclusion in more detail, the following numerical study has been performed. Firstly, a moving jam is induced in a metastable free flow downstream of an on-ramp bottleneck through the use of an initial simultaneous vehicle deceleration of two adjacent vehicles (one vehicle in the left lane and another one in the right lane) with the deceleration -1 m s^{-2} applied during a time interval $T^{(\mathrm{pert})}$ (figure 8, left). An application of the microscopic criterion to this moving jam shows (figure 8(*b*)–(*g*), left) that there is no traffic interruption within the jam. In this case, we find $I_{\mathrm{s}} = \tau_{\max}/\tau_{\mathrm{del}}^{(\mathrm{ac})} < 3$ (model time delay $\tau_{\mathrm{del}}^{(\mathrm{ac})} \approx 1.74$ s). Rather than the moving jam propagates through the bottleneck while maintaining the downstream jam front, this jam is pinned at the bottleneck leading to an F $\rightarrow$ S transition with subsequent localized SP (LSP) formation upstream of the bottleneck (figure 8(*a*), left). In accordance with the phase definition through the macroscopic spatiotemporal objective criteria of the phases in congested traffic (section 1), this jam is a narrow moving jam and the jam is associated with the synchronized flow phase.

Secondly, another moving jam is induced applying a longer perturbation duration $T^{(\mathrm{pert})}$ downstream of the bottleneck (figure 8(*a*), right). However, there is flow interruption within this jam (figure 8(*b*)–(*g*), right). Accordingly to the microscopic criterion for the phases in congested traffic, this jam is a wide moving jam. In this case, we find $I_{\mathrm{s}} \approx 9$ (in the left lane) and 16 (in the right lane). In contrast with former narrow moving jam, this jam propagates through the bottleneck while maintaining the mean downstream jam front velocity (figure 8(*a*), right). As in empirical observations [1], wide moving jam propagation through metastable free flow state at the bottleneck leads to LSP formation as in the case of the former narrow moving jam. In contrast with the narrow moving jam, synchronized flow within the LSP has no influence on wide moving jam propagation (figure 8(*a*), right).

At each of the various chosen values $T^{(\mathrm{pert})}$, many realizations of jam propagation have been performed. It turns out that the duration of flow interruption within a moving jam exhibits fluctuations in the different realizations near an average value $\tau_{\max}$ that depends on $T^{(\mathrm{pert})}$. When $I_{\mathrm{s}} = \tau_{\max}/\tau_{\mathrm{del}}^{(\mathrm{ac})} < 3$, then in all realizations a moving jam is pinned at the bottleneck, i.e., the jam is associated with the synchronized flow phase. In contrast, when $I_{\mathrm{s}} > 5$, then in all realizations a moving jam propagates through the bottleneck, i.e., this jam is associated with the wide moving jam phase. When $3 < I_{\mathrm{s}} < 5$, then in some of the realizations a moving jam is associated with synchronized flow but in the others with a wide moving jam. This can be explained by fluctuations within the jam, in the jam inflow and outflow, as well as fluctuations through random vehicle lane changing. In particular, it can turn out that within a moving jam a vehicle changes lane before it passes the detector. Then a time headway measured by the detector increases. This random lane changing has obviously no relation to flow

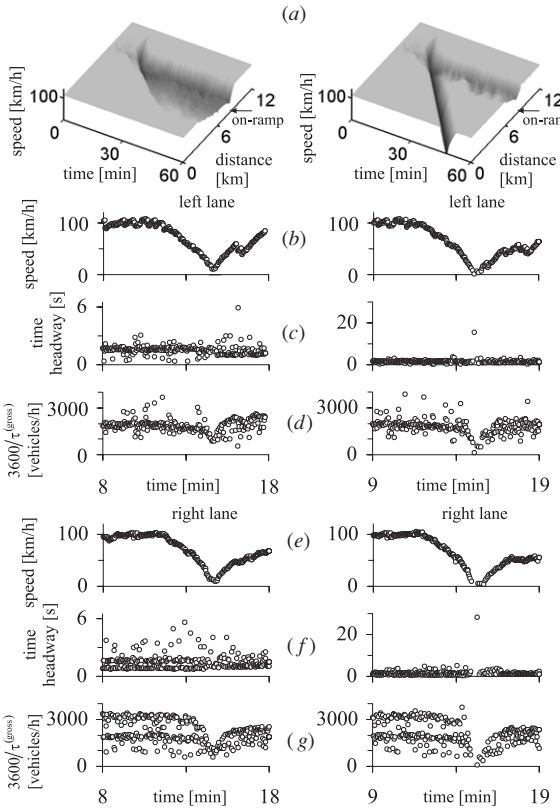

Figure 8. Comparison of microscopic criterion with macroscopic spatiotemporal objective criteria for the phases in congested traffic of identical vehicles. Left figures are related to a narrow moving jam. Right figures are related to a wide moving jam. (*a*) Catch effect of the narrow moving jam at an on-ramp bottleneck with subsequent LSP formation (left), and wide moving jam propagation through the bottleneck with LSP formation (right). Vehicle speed on the main road in space and time that is averaged across two lanes. (*b*), (*e*) Single vehicle data for speed in the left (*b*) and in right lanes (*e*). (*c*), (*d*), (*f*), (*g*) Time headways (*c*), (*f*) and values $3600/\tau^{(\mathrm{gross})}$ (*d*), (*g*) associated with (*b*) and (*e*), respectively. $q_{\mathrm{in}} = 1830$, $q_{\mathrm{on}} = 270$, $q_{\mathrm{out}} = 1810$ vehicles/h/lane. On-ramp location is $x_{\mathrm{on}} = 8.2$ km, on-ramp merging region length is $L_{\mathrm{m}} = 300$ m. Data in (*b*)–(*g*) are related to a location 50 m downstream of the end of the on-ramp merging region. Durations $T^{(\mathrm{pert})}$ of local perturbations and their locations $\Delta x^{(\mathrm{pert})}$ downstream of the end of the on-ramp merging region are (30 s, 660 m) for left figures and (35 s, 820 m) for right figures. Perturbations start at $t_0^{(\mathrm{pert})} = 10$ min. Model of section 16.3 of [1].

interruption within a moving jam. A more detailed study of fluctuations is beyond the scope of this paper.

If durations of vehicle deceleration $T^{(\mathrm{pert})}$ within an initial disturbance causing jam emergence are chosen to be different for a vehicle in the left lane and for a vehicle in the right lane, then flow interruption can occur in the left lane only (figure 9, left) or in the right lane only (figure 9, right). The criterion for a wide moving jam is also valid in these asymmetric cases; however, at greater values $I_{\mathrm{s}} = \tau_{\max}/\tau_{\mathrm{del}}^{(\mathrm{ac})}$ than in the symmetric case shown in figure 8. In the example shown in figure 9, it turns out that a moving jam is a wide moving one at $I_{\mathrm{s}} \approx 27$ in figure 9, left and $I_{\mathrm{s}} \approx 9$ in figure 9, right. In general, simulations show that when flow interruption occurs within a moving jam in the right lane only, then for jam propagation

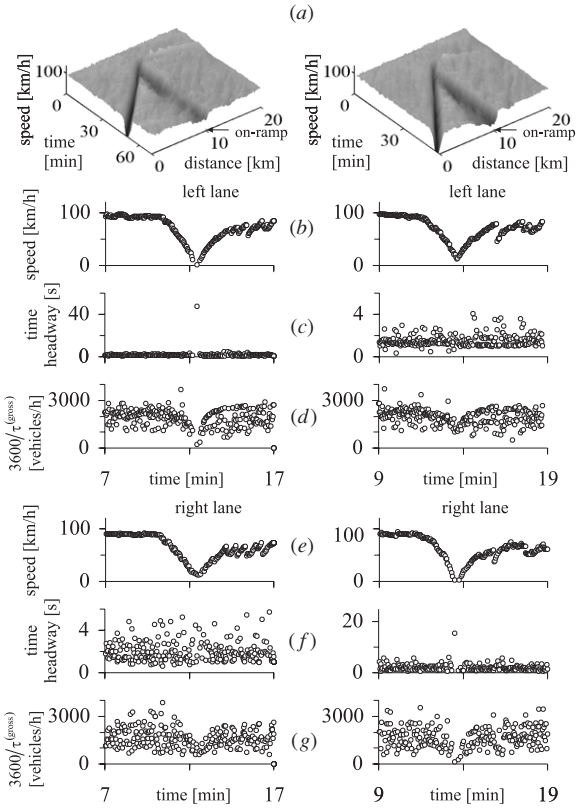

Figure 9. Comparison of microscopic criterion with macroscopic spatiotemporal objective criteria for the phases in congested heterogeneous traffic. Left figures are related to the case in which flow interruption occurs in the left lane and it does not occur in the right lane. Right figures are related to the opposite case in which flow interruption does not occur in the left lane and it does occur in the right lane. (*a*) Wide moving jam propagation through the bottleneck. Vehicle speed in the left lane in space and time. (*b*), (*e*) Single vehicle data for speed in the left (*b*) and right lanes (*e*). (*c*), (*d*), (*f*), (*g*) Time headways (*c*), (*f*) and values $3600/\tau^{(\mathrm{gross})}$ (*d*), (*g*) associated with (*b*) and (*e*). Model for heterogeneous traffic of section 20.2 in [1]; $\tau_{\mathrm{del}}^{(\mathrm{a,j})}(v) = \tau/p_0^{(j)}(v)$, $p_0^{(j)}(v) = a^{(j)} + b^{(j)}\min(1, v/10)$, $j = 1, 2, 3$; $a^{(1)} = 0.565, b^{(1)} = 0.085$ for fast vehicles ($j = 1$), $a^{(2)} = 0.42, b^{(2)} = 0.13$ for slow vehicles ($j = 2$), and $a^{(3)} = 0.3, b^{(3)} = 0.18$ for long vehicles ($j = 3$). 80% fast and 20% long vehicles. $q_{\mathrm{in}} = 1565$, $q_{\mathrm{on}} = 337$ vehicles/h/lane. $q_{\mathrm{out}} = 1900$ and $q_{\mathrm{out}} = 1100$ vehicles/h in the left and right lanes, respectively. Parameters of local perturbations $T^{(\mathrm{pert})}$ and $\Delta x^{(\mathrm{pert})}$ are for left figures (27 s, 450 m) in the left and (25 s, 450 m) in right lanes; for right figures (20 s, 700 m) in the left and (30 s, 700 m) in right lanes. $x_{\mathrm{on}} = 10$ km. Other parameters are the same as those in figure 8.

through the bottleneck (the jam is a wide moving one) a smaller value I_{s} is required than a value I_{s} required for the case of another jam propagation through the bottleneck when flow interruption occurs within this wide moving jam in the left lane only.

3.2. Empirical test of congested pattern characteristics in microscopic three-phase traffic theory

Single vehicle data associated with GP simulations at the bottleneck are compared with empirical results. However, the GP in figure 5 exists about 2 h only. In order to make more

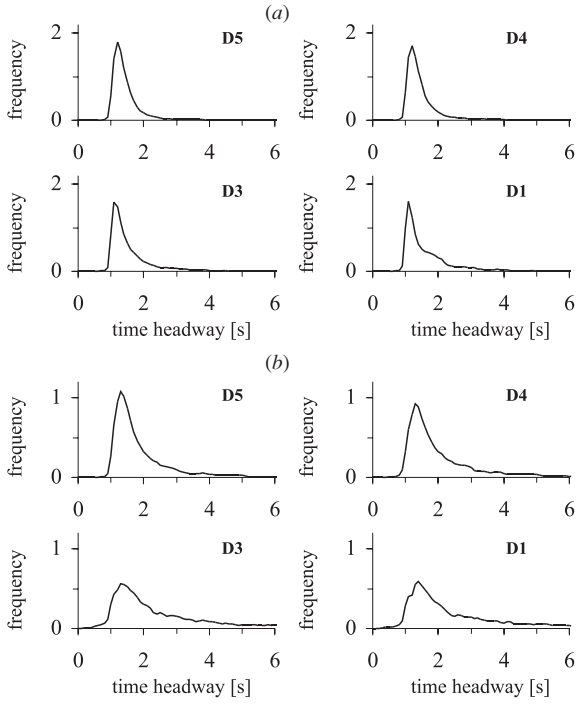

Figure 10. Simulated time headway distributions at different detectors within general patterns. (*a*) Simulations of the model of identical vehicles related to figure 5(*e*). (*b*) Simulations of the model for heterogeneous flow with various driver and vehicle characteristics of section 20.2 in [1] with 30% of fast, 35% of slow and 35% of long vehicles; model parameters are given in the caption to figure 9.

reliable statistical characteristics, after the flow rates $q_{\text{on}}(t)$ and $q_{\text{in}}(t)$ taken from measurements reach their maximum values, these flow rates do not change in simulations any more. Then an GP that occurs at the bottleneck does not dissolve over time at all. The characteristics of this GP are the same as those for the GP in figure 5(*c*)–(*e*) before 7:30.

Time headway distributions related to synchronized flow (D5, D4, figure 10(*a*)) are qualitatively the same as empirical ones (figure 3). However, in the model of identical vehicles used in figure 10(*a*), driver time delays are more close to aggressive drivers. This explains why in synchronized flow longer time headways do not appear in figure 10(*a*). Real traffic is heterogeneous with different vehicle and driver characteristics. When a model of heterogeneous traffic of section 20.2 in [1] is used, then a quantitative correspondence with empirical results of time headway distributions (figure 3) through the appropriate choice of driver and vehicle characteristics is possible (figure 10(*b*)).

Simulated OV functions (figure 11(*a*)) show the same characteristics as those for the empirical OV functions (figure 4). The same conclusion can be drawn for the KKW CA model [16]. For the KKW CA model, OV functions (figure 11(*c*)) have been simulated at the same locations as those in figure 5(*a*) for different congested states within an GP that emerges at the on-ramp bottleneck (figure 11(*b*)). As follows from figure 11(*c*), OV functions presented in [25] with the reference to the KKW CA model are not associated with the KKW CA model. Thus, conclusions about microscopic features of the KKW CA model made in [25] are incorrect.

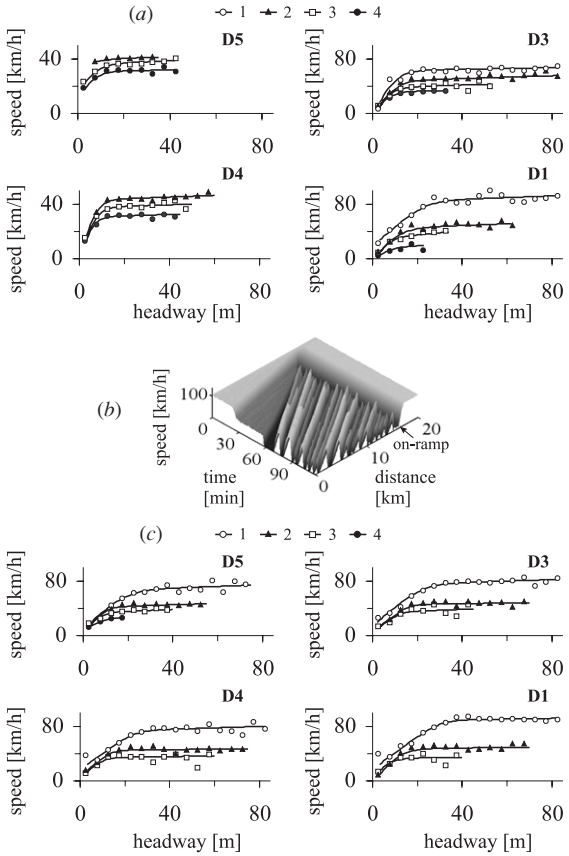

Figure 11. Simulated OV functions at different detectors within general patterns. (*a*) Simulations of the model of identical vehicles related to figure 5(*e*). (*b*, *c*) Simulations of an GP (*b*) and associated OV functions (*c*) for the KKW CA model (section 16.2 in [1]). Curves 1–4: $\rho = 20$–30, $\rho = 30$–40, $\rho = 40$–50, and $\rho = 50$–60 vehicles/km, respectively. In (*b*, *c*), $q_{\text{in}} = 2230$, $q_{\text{on}} = 500$ vehicles/h.

In a study of empirical single vehicle data [34, 35], it has been found that in congested traffic distributions $p_{\delta v}(\delta v)$ for vehicle speed difference $\delta v = v_{i+1} - v_i$ associated with two vehicles i and $i + 1$, which are registered at a detector location one after another, have a very sharp maximum at $\delta v = 0$: there is an attraction of vehicles to a region with a very small speed difference in congested traffic. This behaviour has been explained by the speed adaptation effect in [18, 1]. This effect is found in numerical simulations at D5 and D4 at which synchronized flow without wide moving jams occurs (figure 12(*a*)). However, when wide moving jams appear (D3–D1), then at a given vehicle space headway range the width of frequency distribution $p_{\delta v}(\delta v)$ increases: $p_{\delta v}(\delta v)$ is a function of the spatial co-ordinate (figure 12(*a*)). At freeway locations within a congested pattern in which wide moving jams appear (D3–D1, figure 5(*e*)), the distribution $p_{\delta v}(\delta v)$ for the whole space headway range becomes broader than at the locations at which synchronized flow without wide moving jams is realized (D5) (figure 12(*b*), (*c*)). Even though pattern characteristics can be seen at the distribution function $p_{\delta v}(\delta v)$, this function is not sufficient to characterize the traffic phases. This is because spatiotemporal features of the phases in a large data set, which has to be used, get lost.

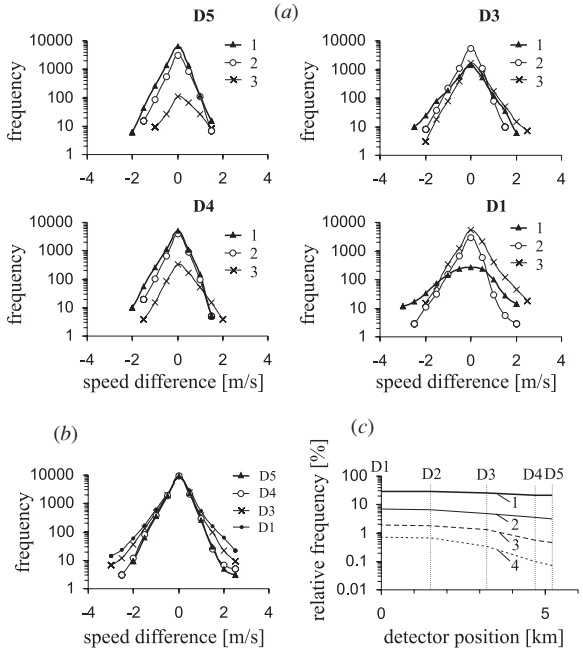

Figure 12. Simulations of speed adaptation effect at different detector locations within the GP in figure 5(*e*): (*a*) Frequency $p_{\delta v}$ as a function of δv for different ranges of the space headway; curves 1: 0–12.5 m, curves 2: 12.5–25 m, curves 3: >25 m (densities $\rho > 50$ vehicles/km, $30 < \rho < 50$, and $\rho < 30$ vehicles/km, respectively). (*b*) Frequency $p_{\delta v}$ as a function of δv at different detectors for the whole space headway range. (*c*) Spatial dependence of relative frequency $p_{\delta v}/p_0$ at different given values of the speed difference δv; curve 1: $\delta v = \pm 0.5$ m s^{-1}, curve 2: $\delta v = \pm 1$ m s^{-1}, curve 3: $\delta v = \pm 1.5$ m s^{-1}, curve 4: $\delta v = \pm 2.0$ m s^{-1}. $p_0 = p_{\delta v}\,|_{\delta v=0}$.

Spatial dependences of the fundamental diagrams and speed correlation functions associated with the GP shown in figure 5 are qualitatively the same (figures 13 and 14) as those characteristics in empirical investigations (figures 15.9 and 12.8 in [1]), respectively. In particular, at the on-ramp bottleneck (D6), the fundamental diagram is associated with the Z-shaped speed–flow rate characteristic (figure 13(*b*)) [1]. In figure 13(*c*) at D5, empirical data for the time interval 06:45–8:00 of the strong congestion condition are used only. For this time interval in the pinch region (D5), both in empirical results (D5, figure 13(*c*)) and simulations of the GP shown in figure 5 (D5, figure 13(*d*)) we find that the flow rate is only a weak density function. In figure 13(*c*) at D1, empirical data before 8:00 are considered when the flow rates q_{in} and q_{on} are large (figure 5(*b*)). Then both in empirical results (D1, figure 13(*c*)) and simulations (D1, figure 13(*d*)) within the region of wide moving jams of the GP (D1, figure 5(*e*)) the whole branch for congested traffic C lies on the line J only.

4. Discussion

Based on empirical and simulated results presented, the following conclusions can be made.

(i) The traffic flow interruption effect within the wide moving jam phase, which can be found for real moving jams only in a *microscopic* analysis of the traffic phases in congested traffic, discloses the physical nature of a qualitatively different behaviour of the wide moving jam phase in comparison with the synchronized flow phase. Due to this microscopic effect, a

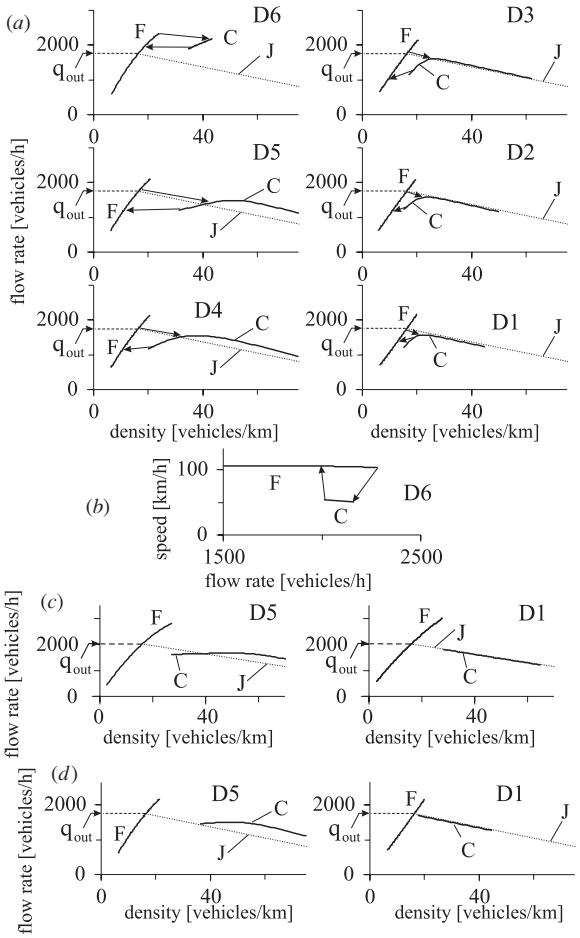

Figure 13. Fundamental diagrams and Z-characteristic. (*a*), (*b*) Simulated spatial dependence of the fundamental diagram (*a*) and the Z-characteristic for the F → S transition at the bottleneck (D6) (b) for the GP shown in figure 5. (*c*) Empirical fundamental diagrams for GP under the strong congestion condition shown in figure 12. 5 of [1] (for D5 time interval 6:45–8:00 and for D1 time interval 7:15–8:00 are used). (*d*) Simulated fundamental diagrams for GP under strong congestion. Arrows in (*a*),(*b*) show F → S transitions (from the branch *F* to the branch *C*) and S → F transitions (from the branch *C* to the branch *F*) at the related detectors. *F*: free flow, *C*: congested traffic. Fundamental diagrams and Z-characteristic are calculated as those in chapter 15 of [1].

wide moving jam propagates through a bottleneck while maintaining the mean velocity of the downstream jam front, whereas a localized region of synchronized flow in which no flow interruption occurs is caught at the bottleneck.

(ii) A microscopic criterion for the wide moving jam phase, which is based on the flow interruption effect, enables us to identify qualitatively different local microscopic congested traffic states in single vehicle data measured at a *single* freeway location.

(iii) Microscopic and macroscopic empirical congested pattern features including the microscopic criterion presented in the paper can be explained by a microscopic three-phase traffic theory of [15–18].

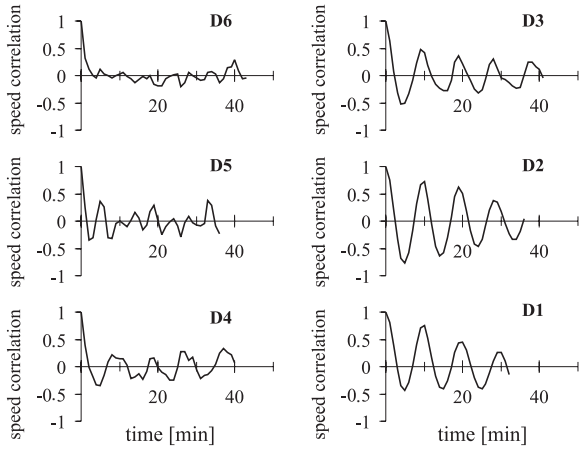

Figure 14. Simulated speed correlation functions at different detectors for the GP in figure 5.

In general, main features of empirical OV functions and time headway distributions are not necessarily qualitatively different, even if local traffic dynamic characteristics within congested patterns are qualitatively different. Therefore, these and many other empirical traffic flow characteristics (e.g., fundamental diagrams, hysteresis effects, etc) could be considered secondary ones in comparison to spatiotemporal traffic pattern features (item (i)–(iv) of section 1). This is because important spatiotemporal features of phase transitions and congested patterns (item (i)–(iv) of section 1) are *lost* in these and many other macroscopic and microscopic traffic characteristics, which are widely used as the empirical basis for tests of traffic flow models. Thus, it is not justified to use these macroscopic and microscopic characteristics as the *solely empirical basis* for a decision whether a traffic flow model can describe real traffic flow or not. In particular, this explains why the Nagel-Schreckenberg CA model and its variants [36] show empirical fundamental diagrams, empirical OV functions and time headway distributions satisfactory [25], even though the NaSch CA models [36] as found in [1, 16] cannot show and predict the main empirical spatiotemporal features of phase transitions in traffic flow and congested traffic patterns (features (i)–(iv) of section 1).

References

[1] Kerner B S 2004 *The Physics of Traffic* (Berlin: Springer)
[2] Gartner N H, Messer C J and Rathi A (ed) 1997 *Special Report 165: Revised Monograph on Traffic Flow Theory* (Washington, DC: Transportation Research Board)
[3] Wolf D E 1999 *Physica* A **263** 438
[4] Chowdhury D, Santen L and Schadschneider A 2000 *Phys. Rep.* **329** 199
[5] Helbing D 2001 *Rev. Mod. Phys.* **73** 1067–141
[6] Nagatani T 2002 *Rep. Prog. Phys.* **65** 1331–86
[7] Nagel K, Wagner P and Woesler R 2003 *Oper. Res.* **51** 681–716
[8] Mahnke R, Kaupužs J and Lubashevsky I 2005 *Phys. Rep.* **408** 1–130
[9] Mahmassani H S (ed) 2005 Transportation and traffic theory: Flow, Dynamics and Human Interaction *Proc. 16th Int. Symp. on Transportation and Traffic Theory* (Amsterdam: Elsevier)
[10] Helbing D, Herrmann H J, Schreckenberg M and Wolf D E (ed) 2000 *Traffic and Granular Flow' 99* (Heidelberg: Springer)
[11] Fukui M, Sugiyama Y, Schreckenberg M and Wolf D E (ed) 2003 *Traffic and Granular Flow' 01* (Heidelberg: Springer)

[12] Hoogendoorn S P, Luding S, Bovy P H L, Schreckenberg M and Wolf D E (ed) 2005 *Traffic and Granular Flow' 03* (Heidelberg: Springer)
[13] Kerner B S 1998 *Phys. Rev. Lett.* **81** 3797
[14] Kerner B S 2002 *Phys. Rev.* E **65** 046138
[15] Kerner B S and Klenov S L 2002 *J. Phys. A: Math. Gen.* **35** L31
[16] Kerner B S, Klenov S L and Wolf D E 2002 *J. Phys. A: Math. Gen.* **35** 9971–10013
[17] Kerner B S and Klenov S L 2003 *Phys. Rev.* **68** 036130
[18] Kerner B S and Klenov S L 2004 *J. Phys. A: Math. Gen.* **37** 8753–88
[19] Davis L C 2004 *Phys. Rev.* E **69** 016108
[20] Lee H K, Barlović R, Schreckenberg M and Kim D 2004 *Phys. Rev. Let.* **92** 238702
[21] Jiang R and Wu Q S 2004 *J. Phys. A: Math. Gen.* **37** 8197–213
[22] Jiang R and Wu Q S 2005 *Euro. Phys. J.* B **46** 581–4
[23] Neubert L, Santen L, Schadschneider A and Schreckenberg M 1999 *Phys. Rev.* E **60** 6480
[24] Knospe W, Santen L, Schadschneider A and Schreckenberg M 2002 *Phys. Rev.* E **65** 056133
[25] Knospe W, Santen L, Schadschneider A and Schreckenberg M 2004 *Phys. Rev.* E **70** 016115
[26] Cowan R J 1976 *Trans. Rec.* **9** 371–5
[27] Koshi M, Iwasaki M and Ohkura I 1983 *Procs. 8th Inter. Sym. on Transportation and Traffic Theory* ed V F Hurdle *et al* (Toronto, Ont: University of Toronto Press) pp 403
[28] Luttinen T 1992 *Transportation Res. Rec.* **1365** 92–8
[29] Bovy P H L (ed) 1998 *Motorway Analysis: New Methodologies and Recent Empirical Findings* (Delft: Delft University Press)
[30] Tilch B and Helbing D 2000 *Traffic and Granular Flow' 99* ed D Helbing, H J Herrmann, M Schreckenberg and D E Wolf (Heidelberg: Springer) p 333
[31] Banks J 2004 *Trans. Rec.* B **37** 539–54
[32] Gurusinghe G S, Nakatsuji T, Azuta Y, Ranjitkar P and Tanaboriboon Y 2003 *Preprints of the 82nd TRB Annual Meeting* TRB Paper No.: 03-4137 (Washington, DC: TRB)
[33] Kerner B S, Klenov S L and Hiller A 2005 *Preprint* physics/0507094
[34] Wagner P and Lubashevsky I 2003 *Preprint* cond-mat/0311192
[35] Wagner P 2003 *Traffic and Granular Flow' 01* ed M Fukui, Y Sugiyama, M Schreckenberg and D E Wolf (Heidelberg: Springer) pp 15–27
[36] Nagel K and Schreckenberg M 1992 *J. Phys. (France)* I **2** 2221
Nagel K and Paczuski M 1995 *Phys. Rev.* E **51** 2909
Schreckenberg M, Schadschneider A, Nagel K and Ito N 1995 *Phys. Rev.* E **51** 2939
Barlović R, Santen L, Schadschneider A and Schreckenberg M 1998 *Eur. Phys. J.* B **5** 793
Knospe W, Santen L, Schadschneider A and Schreckenberg M 2000 *J. Phys. A: Math. Gen.* **33** L477